The Astrophysical Journal, 639:1166–1176, 2006 March 10

IRS SPECTRA OF SOLAR-TYPE STARS: A SEARCH FOR ASTEROID BELT ANALOGS

C. A. Beichman,[1,2] A. Tanner,[2] G. Bryden,[2] K. R. Stapelfeldt,[2] M. W. Werner,[2] G. H. Rieke,[3] D. E. Trilling,[3] S. Lawler,[1] and T. N. Gautier[2]

Received 2005 August 20; accepted 2005 November 7

ABSTRACT

We report the results of a spectroscopic search for debris disks surrounding 41 nearby solar-type stars, including eight planet-bearing stars, using the Infrared Spectrometer (IRS) on the *Spitzer Space Telescope*. With the accurate relative photometry of the IRS between 7 and 34 μm we are able to look for excesses as small as $\sim$2% of photospheric levels, with particular sensitivity to weak spectral features. For stars with no excess, the 3 σ upper limit in a band at 30–34 μm corresponds to $\sim$75 times the brightness of our zodiacal dust cloud. Comparable limits at 8.5–13 μm correspond to $\sim$1400 times the brightness of our zodiacal dust cloud. These limits correspond to material located within the $<$1 to $\sim$5 AU region that, in our solar system, originates predominantly from debris associated with the asteroid belt. We find excess emission longward of $\sim$25 μm from five stars, of which four also show excess emission at 70 μm. This emitting dust must be located in a region starting around 5–10 AU. One star has 70 μm emission but no IRS excess. In this case, the emitting region must begin outside 10 AU; this star has a known radial velocity planet. Only two stars of the five show emission shortward of 25 μm, where spectral features reveal the presence of a population of small, hot dust grains emitting in the 7–20 μm band. One of these stars, HD 72905, is quite young (300 Myr), while the other, HD 69830, is older than 2 Gyr. The data presented here strengthen the results of previous studies to show that excesses at 25 μm and shorter are rare: only 1 out of 40 stars older than 1 Gyr or $\sim$2.5% shows an excess. Asteroid belts 10–30 times more massive than our own appear are rare among mature, solar-type stars.

Subject headings: circumstellar matter — comets: general — Kuiper Belt — minor planets, asteroids — planetary systems

1. INTRODUCTION

The infrared excess associated with main-sequence stars (Aumann et al. 1984) is produced by dust orbiting at distances ranging from $<$1 to $>$100 AU. In discussing these debris disks we often use the analogy of our solar system, where dust is generated by collisions between larger bodies in the asteroid and Kuiper belts, as well as by emission from outgassing comets. As in the solar system, we distinguish between (1) hot (200–500 K) debris located relatively close to the star ($<$1 AU out to $\sim$5 AU) and arising in a region dominated by refractory material, e.g., debris associated with an asteroid belt (Dermott et al. 2002); and (2) cooler debris ($<$30–200 K) located beyond 5 AU that may be associated with more volatile, cometary material, i.e., the analog of our Kuiper Belt. Observed dust luminosities range from $L_{\rm dust}/L_\star \simeq 10^{-5}$ to greater than 10^{-3} for main-sequence stars, compared to $L_{\rm dust}/L_\star \simeq 10^{-7}$ to 10^{-6} inferred for our own Kuiper Belt (Stern 1996; Backman et al. 1995) and $\sim 10^{-7}$ measured for our asteroid belt (Backman & Paresce 1993; Dermott et al. 2002).

The FGK survey of solar-type stars is a *Spitzer* GTO program designed to search for excesses around a broad sample of 148 nearby, F5–K5 main-sequence field stars, sampling wavelengths from 7 to 34 μm with the Infrared Spectrograph (IRS; Houck et al. 2004) and 24 and 70 μm with the Multiband Imaging Photometer for *Spitzer* (MIPS; Rieke et al. 2004). In the context of our paradigm, IRS is well suited to searching for and characterizing hot dust in an asteroid belt analog, while MIPS is better suited to studying cooler material in a Kuiper Belt analog. The sample consists of two components—stars with planets and those without. The MIPS observations of planet-bearing stars are discussed in Beichman et al. (2005a) and of non–planet-bearing stars in Bryden et al. (2006). This paper presents the results of the IRS survey of a subsample of 39 stars, seven with planets and the remainder without planets, based on current knowledge from radial velocity programs. In addition, the paper includes IRS follow-up observations of two stars (one of which is planet-bearing) that were not originally scheduled for spectroscopy, but which were found to have a 70 μm excess. Results for one star with a notable IRS spectrum, HD 69830, have been presented elsewhere (Beichman et al. 2005b) but is summarized below in the context of the complete survey.

The IRS portion of the program was designed with four goals in mind: (1) to extend the wavelength coverage beyond that possible with MIPS to look for dust emitting either shortward or longward of MIPS's 24 μm band; (2) to take advantage of IRS's broad wavelength coverage to reduce systematic errors and thus, possibly, identify smaller excesses than previously possible; (3) to constrain the spatial distribution of dust grains by assessing the range of temperatures present in a given debris disk; and (4) to search for mineralogical features in the spectra of any excesses. In this paper we describe the sample of stars (§ 2); present our calibration procedure and give the reduced spectra for each star (§ 3 and the Appendix); discuss detections of or limits to IR excesses (§ 4); present models of the excesses in the four stars with IRS and MIPS 70 μm excesses and discuss the nature of their debris disks; and discuss overall results and conclusions (§§ 5 and 6).

2. THE SAMPLE

The details of the sample are presented in Bryden et al. (2006). In brief, the survey consists of solar-type stars with main-sequence spectral types ranging from F5 to K5, most of which are within roughly 25 parsecs. Some stars at larger distances were included because they were known to possess planets via radial velocity

[1] Michelson Science Center, California Institute of Technology, M/S 100-22, Pasadena, CA 91125; chas@pop.jpl.nasa.gov.
[2] Jet Propulsion Laboratory, 4800 Oak Grove Drive, Pasadena, CA 91109.
[3] Steward Observatory, University of Arizona, 933 North Cherry Avenue, Tucson, AZ 85721.

TABLE 1
AN IRS SURVEY OF F, G, AND K STARS

Star[a]	Name	Spectral Type	V (mag)[b]	Distance (pc)	AOR	MIPS Excess[c]	IRS Excess[d]
HD 693	GJ 10	F5 V	3.51	18.9	4008448	No, new	
HD 3795	GJ 799	G3 V	3.86	28.6	4009216	N/A	
HD 4628		K2 V	6.41	7.4	4009984	No	
HD 7570	GJ 55	F8 V	4.07	15.1	4010240	70 μm	Long
HD 9826[e]	υ And	F8 V	4.09	13.5	4010496	No, new	
HD 10800	GJ 67.1	G2 V	3.71	27.1	4010752	No	
HD 39091[e]	GJ 9189	G1 V	5.67	18.2	4015616	No	
HD 43834	GJ 231	G6 V	5.05	10.2	4015872	No	
HD 55575	GJ 1095	G0 V	4.42	16.9	4016128	No	
HD 58855	GJ 9234	F6 V	3.87	19.9	4016384	No	
HD 69830	GJ 302	K0 V	5.45	12.6	4016640	24 μm	Short, long
HD 72905	GJ 311	G1.5 V	4.93	13.8	4016896	70 μm	Short, long
HD 75732[e]	ρ (55) Cnc A	G8 V	5.95	12.5	4017152	No	
HD 76151		G3 V	5.74	11.3	4017408	70 μm	Long
HD 84737	GJ 368	G0.5 Va	3.77	18.4	4017664	No	
HD 86728	GJ 376	G3 Va	4.53	14.9	4017920	No, new	
HD 95128[e]	47 UMa	G1 V	5.1	14.1	4018432	No	
HD 101501	GJ 434	G8 Ve	5.43	9.5	4018944	No	
HD 120136[e]	τ Boo	F6 IV	4.5	15.6	4021760	No	
HD 133002	GJ 3876	F9 V	2.46	43.3	4022272	No	
HD 136064	GJ 580.2	F8 V	3.11	25.3	4022784	No	
HD 142373	GJ 602	F9 V	3.61	15.8	4023040	No	
HD 146233		G1 V	4.56	15.4	4081920	No	
HD 154088	GJ652	G8I V–V	5.3	18.1	4029952	No, new	
HD 166620		K2 V	6.14	11.1	4023808	No	
HD 168151		F5 V	3.18	23.5	4024064	No	
HD 173667	GJ 9635	F6 V	2.79	19.1	4024320	No	
HD 181321	GJ755	G5 V	4.89	20.9	4030208	No	
HD 185144		K0 V	5.93	5.6	4024576	No	
HD 188376		G5 V	2.82	23.8	4025088	No	
HD 191408	GJ 783A	K3 V	6.41	6.0	4025600	No, new	
HD 196378	GJ 794.2	F8 V	3.2	24.2	4025856	No, new	
HD 203608	γ Pav	F8 V	4.4	9.2	4026368	No	
HD 212330	GJ 857	G3I V	3.76	20.5	4027136	No, new	
HD 216437[e]	ρ Ind	G2.5 IV	6.06	26.5	4084224	No	
HD 217014[e]	51 Peg	G2.5 IV	5.49	15.4	4027648	No, new	
HD 217813		G5	4.72	24.3	4030464	No, new	
HD 222368		F7 V	3.43	13.8	4028416	No, new	
HD 225239	GJ 3002	G2 V	3.28	36.8	4028672	N/A	
Follow-up observations:							
HD 128311[e]	GJ 3860	K0	7.51	16.5	4083712	70 μm	
HD 206860	GJ 836.7	G0 V	4.62	18.4	12719872	70 μm	Long

[a] Two other stars, HD 190248 (AOR 4025344) and HD 209100 (AOR 4026625), were observed as part of this program using the IRS High Resolution mode. These stars will be discussed elsewhere. HD 33262 was not observed properly due to a pointing error and is not considered further.
[b] Spectral types from SIMBAD. Visual magnitudes and distances as quoted in SIMBAD, typically from the *Hipparcos* satellite.
[c] Star either does or does not have 24 or 70 μm excess as observed by MIPS. "New" means that MIPS data were obtained subsequently to data presented in Beichman et al. (2005a) or Bryden et al. (2006) and are described in Table 3. "N/A" means that the star has not yet been observed with MIPS due to scheduling constraints.
[d] Star has excess as observed by IRS as described in this paper at either short (8–13 μm) or long (30–34 μm) wavelengths.
[e] Star has at least one radial velocity planet.

studies (Butler et al. 1999; Marcy et al. 2002). A subsample of 39 stars covering the full range of spectral types was selected for IRS observations. Table 1 describes 41 stars, including follow-up observations of two stars earlier found by MIPS to have excesses (Table 4) (Beichman et al. 2005a; Bryden et al. 2006). Of the 39 original survey stars, seven are known to have planets from radial velocity studies with one additional planet-bearing star (HD128311) selected for follow-up due to a possible MIPS excess. We also report MIPS results obtained after the observations reported in (Beichman et al. 2005a; Bryden et al. 2006) for nine stars in the spectroscopic sample (Table 3); three of the stars observed with IRS have not yet been observed with MIPS due to the as yet incomplete scheduling of the GTO program. Of the nine new stars observed with MIPS, none has a 24 or 70 μm excess.

3. OBSERVATIONS AND DATA REDUCTION

3.1. *IRS Spectra*

We observed each star with the three longest wavelength modules of the IRS: Short-Low Order 1 (SL1; 7.5–14.0 μm), Long-Low Order 2 (LL-2; 14.0–20.5 μm), and Long-Low Order 1 (LL-1, 20–34 μm). The basic observing sequence and associated data reduction have been described in Beichman et al. (2005b) and are reviewed in the Appendix. In summary, we have used the fact that

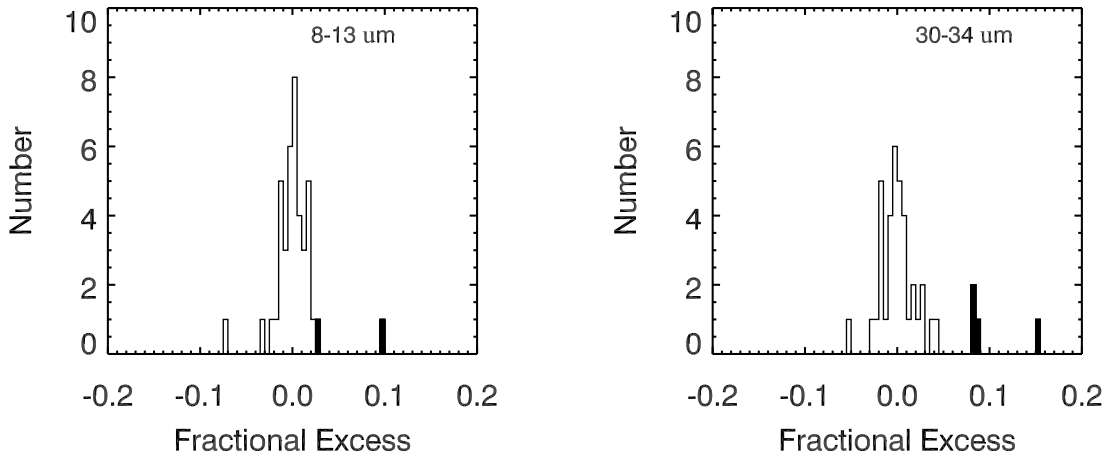

FIG. 1.—Histograms showing the distribution of fractional excess—(observed-photosphere)/photosphere—estimated within pass bands at 8.5–13 (*left*) and 30–34 μm (*right*). The point for HD 69830 is off-scale to the right at 30–34 μm with a relative excess of 0.5. Sources shown with blank bars have statistically significant excesses.

the majority of the sample shows no excess at MIPS wavelengths (24 or 70 μm) or in an initial examination of the IRS data to derive a "superflat" to improve the relative and absolute calibration of all the IRS spectra. After calibration with respect to photospheric models fitted to shorter wavelength ($\lambda < 5$ μm) photometry, the agreement between the *Spitzer* IRS data and the *IRAS* (*Infrared Astronomical Satellite*) and *Spitzer* MIPS photometry is excellent: IRS/*IRAS*(12 μm) = 0.96 ± 0.01; IRS/*IRAS*(25 μm) = 0.93 ± 0.01; and IRS/MIPS(24 μm) = 0.99 ± 0.03.

To look for IR excesses we first examined differences between the flattened, calibrated spectra and photospheric models appropriate to each star (see the Appendix and Bryden et al. 2006). For convenience, we define two "photometric bands" useful for isolating either the silicate features (8.5–13 μm) or a long-wavelength excess (30–34 μm). For all 41 stars in the sample, the average level of the deviation from an extrapolation of the photospheric emission, $[F_\nu(\text{observed})-F_\nu(\text{photosphere})]/F_\nu(\text{photosphere})$, has values of −0.007 ± 0.067 in the 8.5–13 μm band and −0.006 ± 0.066 in the 30–34 μm band. Only HD 69830 (Beichman et al. 2005b) stands out as having a significant excess from this first look at the data.

However, a closer examination of the individual spectra showed that in most cases the data for an individual IRS module differed from the extrapolated photospheric emission in a systematic way that could be attributed to a simple scale or offset error. Without worrying about the source of the scale error (due to either the photospheric extrapolation or residual calibration errors in the IRS spectra), we derived a new calibration factor for each star and for each IRS module using the first 10 points of each module, effectively pinning the IRS spectrum to the photosphere at the short-wavelength end of each of the three IRS modules: SL1 from 7.5 to 8.0 μm; LL-2 from 14.0 to 19.8 μm; and LL-1 from 19.5 to 21 μm. Values of this calibration factor deviated from unity on a star-by-star basis by less than 10%. This technique produced much smaller residuals showing no significant deviations from zero over the entire IRS wavelength range (Figs. 1*a* and 1*b*) for the vast majority of the sample. The dispersion in the deviation from a smooth photosphere was reduced from ~7% to 1.3% (8.5–13 μm) and 1.7% (30–34 μm).[4] A longer wavelength excess beyond the first 10 data points was not affected by the choice of the number of points used to set the normalization. Using this technique, we found no deviation from a stellar photosphere for the majority of stars. However, as described below, we did find clear evidence of an excess rising up at wavelengths longward of ~25 μm in five stars and a silicate feature appearing longward of 8 μm in two stars.

Unlike the other stars in the survey, HD 101501 showed anomalous structure at the few percent level in its spectrum that could not be removed using the normalizations described above. The module-wide deviations from flatness are suggestive of uncorrected flat-field errors, not astrophysical effects. We put an upper limit of 5% of the photospheric emission on any excess for this star. One or two stars, e.g., HD 76151 (Fig. 4), showed small residual offsets of a few mJy between the spectrum and the photosphere in the 8–14 μm band where the star is brightest. As these "features" are at a level less than the ~1.5% dispersion in the excesses averaged over the entire sample, we do not regard them to be significant.

After flattening and normalizing the IRS spectra as described above, we estimated the fractional excess $[F_\nu(\text{observed})-F_\nu(\text{photosphere})]/F_\nu(\text{photosphere})$. Figure 1 gives histograms of the fractional excess estimated in 8.5–13 and 30–34 μm "pass bands." In assessing the significance of an excess we looked at the internal uncertainty in the flux density measurement of a given star and the fractional excess relative to the ~1.5% dispersion of the entire sample (Table 2). Typically, the uncertainty in the fractional excess relative to the population as a whole is more important in assessing the reality of a spectral feature. There are a number of stars that appear to have a significant excess when looking only at the internal uncertainties in flux density, but which are not so impressive when compared to the dispersion in the overall population. If we require any excess to be more significant than 3 times the population-averaged dispersion (1.3% [8–13 μm] and 1.7% [30–34 μm]; Fig. 1), then based on the data presented in Table 2 we can claim statistically significant 30–34 μm excesses for five stars (HD 7570, HD 69830, HD 72905, HD 76151, and HD 206860). One star, HD 69830, shows a highly significant silicate feature starting around 8 μm. Four of these sources, but not HD 69830, also show a 70 μm excess. In the case of HD 72905, which also shows a 70 μm excess, its 8–13 μm flux density excess is highly significant relative to internal uncertainties (12 σ), its fractional excess (2.8%) is modestly significant (2.2 σ) relative to the dispersion in the population, and the spectrum (discussed below)

[4] We also examined a star-by-star normalization factor derived using the entire module, not just the first 10 points. This choice resulted in a similar reduction in dispersion but had deleterious effects on the few sources identified with excesses rising to longer wavelengths.

TABLE 2
IRS Excess in 8.5–13 and 30–34 μm Bands

Star	8.5–13 μm				30–34 μm			
	Excess (mJy)	Fractional Excess	Excess/ Dispersion[a]	$L_{dust}/L_\star$[b] ($\times 10^{-5}$)	Excess (mJy)	Fractional Excess	Excess/ Dispersion[a]	$L_{dust}/L_\star$[b] ($\times 10^{-5}$)
HD 693	-20.8 ± 1.3	-0.015	-1.2	<8.2	0.3 ± 0.8	0.002	0.1	<0.4
HD 3795	-5.5 ± 0.5	-0.008	-0.7	<13	-1.9 ± 0.6	-0.026	-1.3	<0.7
HD 4628	13.8 ± 0.9	0.009	0.7	<26.8	-0.8 ± 1.3	-0.004	-0.2	<1.4
HD 7570	4.4 ± 0.5	0.004	0.3	<9.7	10.7 ± 0.9	0.082	4.3	0.8
HD 9826	-7.4 ± 0.9	-0.003	-0.3	<9.7	-1.3 ± 1.5	-0.004	-0.2	<0.5
HD 10800	8.8 ± 0.3	0.015	1.2	<13	-1.6 ± 0.8	-0.024	-1.1	<0.7
HD 39091	7.4 ± 0.4	0.010	0.8	<13	0.0 ± 3.3	-0.006	-0.1	<0.7
HD 43834	0.1 ± 0.6	-0.001	0.0	<13.9	0.5 ± 0.9	0.004	0.2	<0.7
HD 55575	4.1 ± 0.5	0.006	0.4	<11.1	0.8 ± 0.9	0.008	0.4	<0.6
HD 58855	3.1 ± 0.5	0.005	0.4	<9.7	-0.4 ± 0.9	-0.004	-0.2	<0.5
HD 69830[c]	72.3 ± 4.5	0.099	7.0	41.6	42 ± 1	0.50	24.4	8.0
HD 72905	22.3 ± 1.2	0.028	2.2	9.5	7.0 ± 0.5	0.083	4.5	1.1
HD 75732	14.4 ± 0.5	0.019	1.5	<13.9	1.5 ± 0.9	0.019	0.9	<0.7
HD 76151	10.0 ± 0.3	0.018	1.4	<13	10.1 ± 0.7	0.151	7.3	2
HD 84737	21.1 ± 0.6	0.017	1.4	<11.1	-0.3 ± 1.1	-0.002	-0.1	<0.6
HD 86728	-13.7 ± 0.7	-0.012	-0.9	<13	0.1 ± 0.8	0.002	0.1	<0.7
HD 95128	-28.1 ± 0.9	-0.022	-1.7	<11.1	0.6 ± 1.3	0.006	0.3	<0.6
HD 101501[d]	-98.4 ± 1.8	-0.071	-5.6	<13.9	0.6 ± 1.1	0.005	0.3	<0.7
HD 120136	15.8 ± 0.6	0.011	0.8	<9.7	-1.2 ± 1.6	-0.007	-0.3	<0.5
HD 128311	-0.9 ± 0.4	-0.003	-0.2	<16	1.4 ± 0.6	0.037	1.6	<0.8
HD 133002	1.8 ± 0.6	0.002	0.1	<11.1	2.9 ± 1.0	0.025	1.3	<0.6
HD 136064	-6.6 ± 0.6	-0.007	-0.6	<9.7	0.2 ± 1.0	0.002	0.1	<0.5
HD 142373	1.2 ± 0.7	0.001	0.0	<11.1	-3.5 ± 2.0	-0.017	-0.8	<0.6
HD 146233	-28.1 ± 1.2	-0.032	-2.5	<13	-1.6 ± 0.9	-0.018	-0.9	<0.7
HD 154088	-5.3 ± 0.3	-0.013	-1.0	<13.9	-0.6 ± 1.1	-0.017	-0.6	<0.7
HD 166620	-0.3 ± 0.4	0.000	0.0	<26.8	-0.2 ± 0.6	-0.002	-0.1	<1.4
HD 168151	15.7 ± 0.8	0.016	1.3	<8.2	-0.9 ± 0.8	-0.009	-0.5	<0.4
HD 173667	46.4 ± 0.9	0.023	1.8	<9.7	9.7 ± 1.5	0.043	2.3	<0.5
HD 181321	0.3 ± 0.4	0.001	0.1	<13	0.0 ± 0.6	0.002	0.1	<0.7
HD 185144	-5.5 ± 2.1	-0.003	-0.2	<16	3.2 ± 2.0	0.011	0.6	<0.8
HD 188376	12.8 ± 1.1	0.005	0.4	<13	-3.5 ± 2.2	-0.013	-0.7	<0.7
HD 191408	-8.7 ± 1.0	-0.004	-0.3	<26.8	4.4 ± 1.8	0.020	1.0	<1.4
HD 196378	-15.3 ± 1.2	-0.012	-0.9	<9.7	2.1 ± 0.8	0.016	0.8	<0.5
HD 203608	-38.2 ± 0.8	-0.016	-1.3	<9.7	-5.2 ± 1.4	-0.019	-1.0	<0.5
HD 206860	-0.6 ± 0.4	-0.001	-0.1	<11.1	5.3 ± 0.7	0.085	4.0	0.9
HD 212330	16.7 ± 0.8	0.014	1.1	<13	-0.4 ± 0.8	-0.004	-0.2	<0.7
HD 216437	1.0 ± 0.4	0.003	0.2	<13	-1.0 ± 0.3	-0.019	-1.0	<0.7
HD 217014	2.0 ± 0.5	0.002	0.2	<13	-0.7 ± 1.0	-0.008	-0.4	<0.7
HD 217813	0.5 ± 0.3	0.001	0.1	<13	-1.8 ± 1.2	-0.054	-1.4	<0.7
HD 222368	-14.4 ± 1.6	-0.007	-0.5	<9.7	7.0 ± 1.7	0.025	1.3	<0.5
HD 225239	-8.6 ± 0.5	-0.015	-1.2	<13	0.4 ± 0.6	0.005	0.3	<0.7
Average[e]	...	...	...	14 ± 6	...	...	...	0.74 ± 0.31

[a] Excess divided by dispersion averaged over entire sample.
[b] Limits on $L_{dust}/L_\star$ from using eq. (2) and 3 times the dispersion in the fractional excess of the whole population.
[c] Data on excess taken from Beichman et al. (2005b).
[d] Star shows significant flat field errors after recalibration and is not considered further.
[e] Average value of $L_{dust}/L_\star$ (3 σ limits or detections) after 2 σ rejection of outliers.

closely matches that expected for silicate emission. Thus, we regard the 8–13 μm excess of HD 72905 as real.

Figures 2*a*–2*f* shows the IRS spectra for six sources (HD 128311, HD 216437, HD 7570, HD 72905, HD 76151, and HD 206860) plotted in three different ways: (1) their calibrated spectrum; (2) their excess relative to photosphere after normalization with respect to the first 10 points of each module, and (3) the fractional amount of the excess relative to the photosphere after normalization. The dashed lines in the bottom panel show an estimate of the 2 σ dispersion in the deviations from the photospheric models. Fractional deviations between these lines should be regarded with skepticism. The first two stars (HD 128311 and HD 216437) show no apparent excess and are representative of the bulk of the sample. The last four stars (HD 7570, HD 72905, HD 76151, and HD 206860, plus HD 69830, shown in Beichman et al. 2005b) have excesses based on statistical criteria defined above.

3.2. *New MIPS Data*

MIPS observations for nine stars not previously reported (Beichman et al. 2005a; Bryden et al. 2006) are summarized in Table 3. The 24 and 70 μm photometry were derived using processing steps detailed in Bryden et al. (2006) and is based on the DAT software developed by the MIPS instrument team (Gordon et al. 2005). For consistency, we use the same analysis tools and

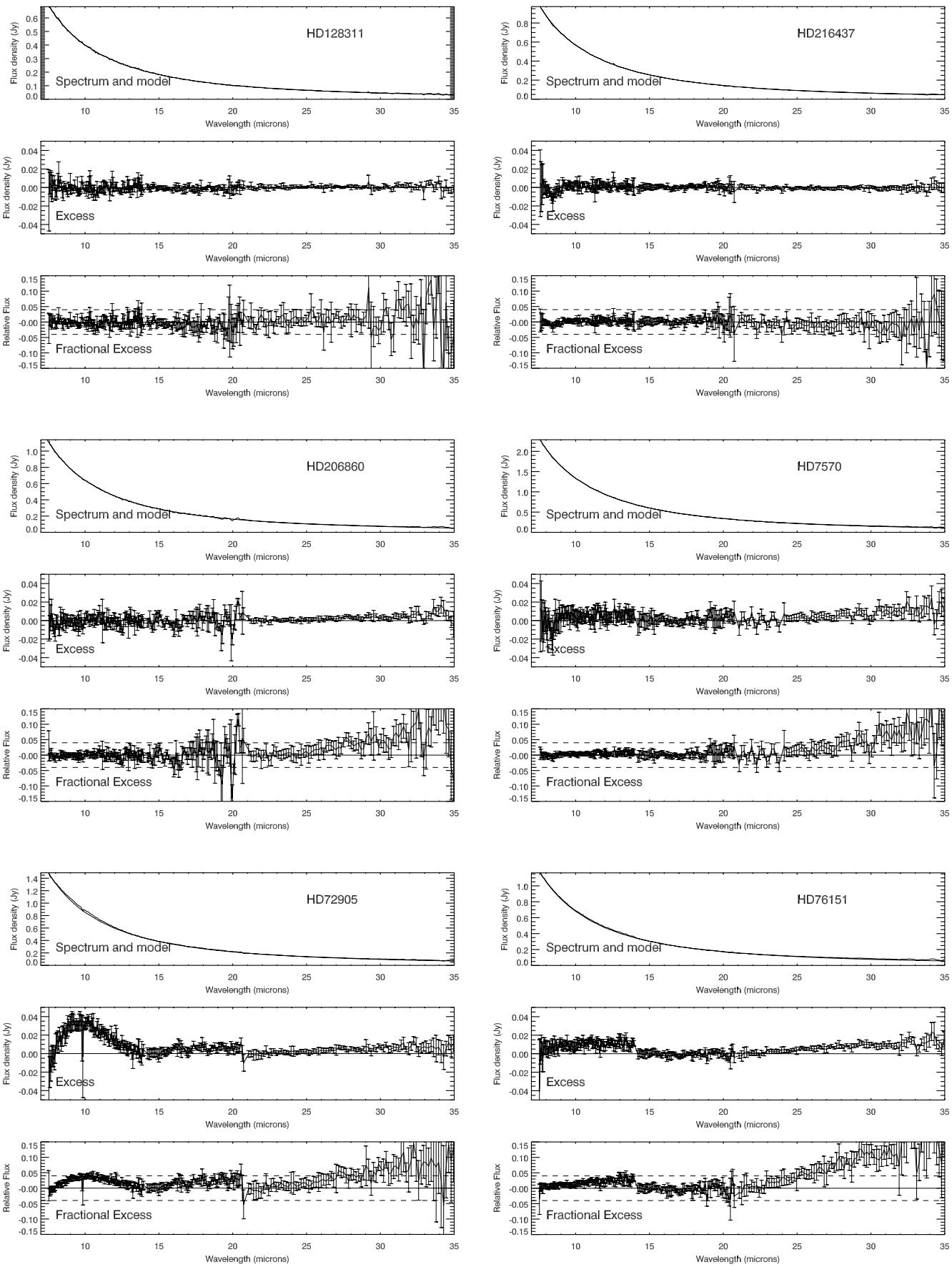

FIG. 2.—IRS spectrum (*top*), excess flux (*middle*), and fractional excess (*bottom*) as a function of wavelength for HD 128311, HD 216437, HD 206860, HD 7570, HD 72905, and HD 76151. The first two stars have *no measurable excess* and are shown as representative of the majority of the sample. Also plotted in the bottom figure are the approximate 2 σ dispersion in the deviations from the photospheric models. Fractional deviations between these lines should be regarded with skepticism.

TABLE 3
NEW MIPS OBSERVATIONS

Star	AOR	F_ν (24 μm)[a] (mJy)	Photosphere[b] (mJy)	Observed/ Photosphere	F_ν (70 μm) (mJy)	Photosphere[b] (mJy)	Observed/Photosphere	$\chi 70$[c]	L_d/L_* (70 μm)
HD 693	4030976	254	265	0.96	37.7 ± 5.6	30.0	1.26	1.37	$<0.4 \times 10^{-5}$
HD 9826[d]	4033280	519	539	0.96	51.2 ± 10.3	60.7	0.84	−0.92	$<0.4 \times 10^{-5}$
HD 154088	4061696	87	70	1.24	−0.1 ± 6.6	7.8	...	−1.19	$<2.7 \times 10^{-5}$
HD 191408	4055040	443	435	1.02	46.7 ± 12.2	50.1	0.93	−0.28	$<1.5 \times 10^{-5}$
HD 196378	4055808	227	254	0.90	30.5 ± 5.6	28.9	1.06	0.29	$<0.4 \times 10^{-5}$
HD 212330	4058368	235	234	1.01	26.4 ± 5.8	26.5	1.00	−0.01	$<0.7 \times 10^{-5}$
HD 217014	4058880	188	178	1.06	25.2 ± 5.3	20.0	1.26	1.00	$<0.2 \times 10^{-5}$
HD 217813	4062464	59	70	0.85	3.7 ± 4.8	7.9	0.47	−0.87	$<1.8 \times 10^{-5}$
HD 222368	4060160	514	534	0.96	54. ± 10.2	60.4	0.91	−0.56	$<0.4 \times 10^{-5}$
Average	...	...	...	1.00 ± 0.04	...	...	0.92 ± 0.09	...	...

NOTE.—MIPS data obtained after data presented in Beichman et al. (2005a) and Bryden (2006).
[a] Statistical noise is negligible.
[b] Photospheric prediction based on extrapolation from 2MASS and shorter wavelength data as described in the text and in Bryden et al. (2006).
[c] We define $\chi 70$ as (observed−photosphere)/noise.
[d] Ups And.

calibration numbers as were adopted by Beichman et al. (2005a) and Bryden et al. (2006).

At 24 μm, we carried out aperture photometry on reduced images using an aperture of 6 camera pixels (1 pixel = 2.″5 at 24 μm) in radius, a background annulus from 12 to 17 pixels, and an aperture correction of 1.15. The flux level is calibrated at 1.047 μJy arcsec^{-2}/(DN s^{-1}), with a default color correction of 1.00 appropriate for sources warmer than 4000 K at a weighted-average wavelength of 23.68 μm.

At 70 μm we used images processed beyond the standard DAT software in order to correct for time-dependent transients, corrections which can significantly improve the sensitivity of the measurements (Gordon et al. 2005). Because the accuracy of the 70 μm data is limited by background noise, we used a relatively small aperture of just 1.5 pixels (1.″5 × 9″) in radius and a 4–8 pixel radius sky annulus. This aperture size requires a relatively high aperture correction of 1.79. The flux level is calibrated at 15,800 μJy arcsec^{-2}/MIPS_70_unit, again with a default color correction of 1.00.

The 24 and 70 μm data are presented in Table 3, which also includes a comparison with the predicted level of photospheric emission based on models fitted to 2MASS (Two Micron All Sky Survey) and shorter wavelength data (Bryden et al. 2006). None of the new objects shows an excess at 24 μm. However, since accurate 2MASS data are not available for most of these bright ($K_s < 6$ mag) stars due to saturation effects, a significant part of the dispersion for the stars studied herein is probably due to the uncertainties in the photospheric extrapolation. We define the parameter $\chi 70 = [F_\nu(\text{observed}) - F_\nu(\text{photosphere})]/\sigma$ at 70 μm, where σ is a combination of internal and calibration uncertainties, as discussed in detail in Bryden et al. (2006). Using $\chi 70$ as a criterion, none of the new objects show a significant 70 μm excess.

The 30–34 μm excess toward the five stars described above (HD 7570, HD 69830, HD 72905, HD 76151, and HD 206860) have been carefully compared with MIPS observations at 24 μm (Bryden et al. 2006). A sample of 87 stars in the FGK survey selected for having no 70 μm excess (MIPS-70/photosphere < 1.5) has a 2 σ clipped average of the MIPS-24/photosphere ratio = 0.978 ± 0.001 with a dispersion of 0.056 (Bryden et al. 2006). HD 69830 is clearly detected as a strong MIPS-24 excess with a MIPS-24/photosphere ∼ 1.5. HD 76151 and HD 206860 have MIPS-24/photosphere ratios of 1.00 and 0.96 and show no evidence for 24 μm excess. HD 72905 and HD 7570 represent intermediate cases, however, with MIPS-24/photosphere ratios of 1.064 and 1.053. While the nominal dispersion for the 24 μm data would suggest that these MIPS-24 excesses are not significant (<2 σ), further analysis of the MIPS data (K. Su 2005, private communication) suggests that the combined photospheric and MIPS uncertainties may be closer to 2%, in which case these modest excesses may turn out to be real. In a similar vein, Bryden et al. (2006) have identified a weak general trend (1.5–2 σ) for stars with 70 μm excesses to have slightly higher MIPS-24/photosphere ratios than for stars without a longer wavelength excesses. If the weak MIPS excesses hinted at here can be made more significant with careful calibration and validation using IRS, then it may be possible to look for weak, warm excesses in a much larger sample of objects than would be possible with IRS alone.

4. RESULTS

4.1. *Statistics of Detections*

We detected significant IRS excess emission in five sources including HD 69830 (Beichman et al. 2005b). Of these five stars, all except HD 69830 also have a MIPS 70 μm excess. Two stars, HD 128311 and HD 206860, were included explicitly for IRS follow-up observations because they had MIPS excess emission. HD 128311 shows no IRS excess,[5] while HD 206860 does show an excess at 30–34 μm. Out of the 39 stars in the initial survey, we have identified 30 μm IRS excesses around four stars (HD 69830, HD 72905, HD 7570, and HD 76151), or 11% ± 5%, which is consistent with the fraction of stars with excesses found at 70 μm (Bryden et al. 2006). Including the two follow-up stars (HD 206860 and HD 128311) brings the detection rate to 5 of 41 stars, or 12% ± 5% at 30 μm. None of the eight planet-bearing stars have 30 μm excesses, a smaller fraction than seen with MIPS 70 μm excesses, <12% versus 24% ± 10% (Beichman et al. 2005a). The result is suggestive of an absence of warm dust at levels detectable by IRS, but is not inconsistent with the expected fraction given the small number statistics.

If we apply a similar analysis to the 8–14 μm portion of the spectrum, the corresponding statistics give detections of just two objects (HD 69830 and HD 72905) out of the 39 stars (with and

[5] The 70 μm detection of HD 128311 (Beichman et al. 2005a) is marginal and awaits confirmation in a pending MIPS observation.

without planets) in the initial survey, or 5.1% ± 3.6%, and zero of eight planet-bearing stars. Removing HD 72905 from the overall statistics because it is quite young, 300 Myr (Spangler et al. 2001) based on its membership in the Ursa Major moving group, reduces the statistics to just one short-wavelength excess out of 38 mature stars (>1 Gyr as discussed in Bryden et al. 2006) or <2.5% in the initial survey. These data confirm the rarity of short-wavelength excesses compared with ones at longer wavelengths. This result was first noted on the basis of *IRAS* and *ISO* (*Infrared Space Observatory*) data (Aumann & Probst 1991; Mannings & Barlow 1998; Fajardo-Acosta et al. 2000; Laureijs et al. 2002) and reconfirmed with MIPS data (Beichman et al. 2005a; Bryden et al. 2006), but is extended here to lower levels of emission, i.e., 2% relative excess for IRS versus 6%–10% for *IRAS* and *ISO*. In the next section we convert these observational limits into a limit on the fractional luminosity of dust in these systems, $L_{\rm dust}/L_\star$.

4.2. *Limits on the Fractional Disk Luminosity,* $L_{\rm dust}/L_\star$

A useful metric for the limits on dust surrounding these stars is L_d/L_*, which is related to the fractional flux limit of an excess relative to the Rayleigh Jeans tail of the star's photosphere (Bryden et al. 2006):

$$\frac{F_{\rm dust}}{F_\star} = \frac{L_{\rm dust}}{L_\star}\frac{h\nu T_\star^3}{kT_{\rm dust}^4(e^{h\nu/kT_{\rm dust}}-1)}, \quad (1)$$

from which it is easy to show that

$$\frac{L_d}{L_*} = \frac{F_{\rm dust}}{F_*}\frac{e^{x_d}-1}{x_d}\left(\frac{T_d}{T_*}\right)^3, \quad (2)$$

where $F_{\rm dust} = F_\nu(\text{observed}) - F_\nu(\text{photosphere})$. At the peak of the blackbody curve $x_d \equiv h\nu/kT_d$ has a constant value of 3.91, corresponding to $T_d = 367$ K at 10 μm. At this wavelength $L_d/L_* = 0.00345[5600\ \text{K}/T_*]^3 F_d/F_*$. In Table 2 and Figure 3, we evaluate $L_{\rm dust}/L_\star$ for each star using the appropriate effective temperature and luminosity (from SIMBAD, Table 1) and its measured fractional excess, $F_{\rm dust}/F_*$, or in the case of an upper limit, 3 $\sigma_{\rm pop}$, where $\sigma_{\rm pop}$ is the dispersion in fractional excess averaged over the whole sample. We calculate these dust limits in the 8.5–13 and 30–34 μm portions of the IRS spectrum assuming $T_d = 367$ and 115 K at 10 and 32 μm, respectively. This definition of $L_{\rm dust}/L_\star$ assumes that the emitting material is all located at the location where the peak of the T_d blackbody matches the wavelength of observation. More emitting dust, and higher values of $L_{\rm dust}/L_\star$, would be required for material located substantially interior or exterior to this point.

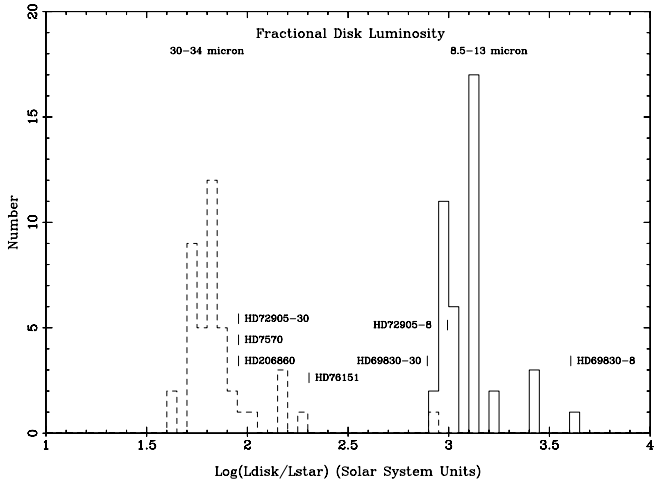

FIG. 3.—Histograms showing the detections or (mostly) 3 σ upper limits on $L_{\rm dust}/L_\star$ for dust emitting in 30–34 μm band (*dashed lines*) and the 8.5–13 μm band (*solid lines*) for the stars in this survey. These limits take into account the effective temperature, $T_{\rm eff}$, and fractional excess for each star as described in the text and are given in units of the solar system's approximate level of zodiacal emission, $L_{\rm dust}/L_\star = 10^{-7}$ (Backman & Paresce 1993). The positions of the positive detections are indicated along with the star's name. An 8 or a 30 is appended to the name to resolve any ambiguity as to which band is being shown. The remainder of the values are upper limits.

TABLE 4
MIPS EXCESSES

Star	F_ν (70 μm) Excess[a] (mJy)	$L_{\rm dust}/L_\star$ (70 μm)	$L_{\rm dust}/L_\star$ (10–70 μm)
HD 7570	14 ± 6	0.38×10^{-5}	0.43×10^{-5}
HD 69830[b]	<3	$<0.5 \times 10^{-5}$	20×10^{-5}
HD 76151	16 ± 4	1.0×10^{-5}	1.2×10^{-5}
HD 72905[c]	24 ± 4	1.2×10^{-5}	2.9×10^{-5}
HD 128311.....	18 ± 4	2.6×10^{-5}	...
HD 206860	15 ± 4	0.92×10^{-5}	0.7×10^{-5}

[a] Bryden et al. (2006).
[b] Beichman et al. (2005b).
[c] The star HD 72905 has a 70 μm flux density of 24 ± 3 mJy (Bryden et al. 2006), a factor of 2–3 lower than measured by ISO-PHOT at 60 and 90 μm (Spangler et al. 2001). We adopt the MIPS value.

The 3 σ limits on $L_{\rm dust}/L_\star$ at 8.5–13 and 30–34 μm have 2 σ clipped average values of $L_{\rm dust}/L_\star = 14 \pm 6 \times 10^{-5}$ and $0.74 \pm 0.31 \times 10^{-5}$, respectively (Table 2). In comparison with our solar system, which has $L_{\rm dust}/L_\star \sim 10^{-7}$ (Backman & Paresce 1993; Dermott et al. 2002), the IRS results set limits (3 σ) on warm (360 K) dust peaking at 10 μm of ~1400 times the level of emission in our solar system. For cooler dust (~120 K) peaking at 30–34 μm, the 3 σ limit corresponds to ~74 times the nominal $L_{\rm dust}/L_\star$ of our zodiacal cloud.

For objects with detections in the IRS bands, we can determine $L_{\rm dust}/L_\star$ explicitly by integrating over the data between 10 and 34 and extrapolating using the models discussed below out to 70 μm. These values are given in Table 4 and are compared with the 70-μm–only estimates obtained using equation (1). Including the IRS spectra increases the estimated $L_{\rm dust}/L_\star$ by about a factor of 1–2 relative to the 70-μm–only estimate. For the nine stars with new upper limits to an excess at 70 μm (Table 3), we also report limits on $L_{\rm dust}/L_\star$.

5. DISCUSSION

5.1. *Models of Disks around Solar-Type Stars*

We fitted the IRS spectra and MIPS 70 μm photometry using a simple model of optically thin dust within one or two flat dust annuli centered around the star. As a guide to subsequent modeling, we first modeled the emission using blackbody grains at a single temperature in equilibrium with the parent star. From the ratio between the 30–34 μm and the 70 μm flux densities for each star we found (Table 5) grain temperatures in the range 75–100 K, with equilibrium distances of 8–14 AU for the four stars. Even though the uncertainties in the flux density ratio are quite large (~25%), the temperature and location of the grains are reasonably well defined, ±1 AU and ±15 K, given the assumption of blackbody grains.

We calculated the power-law temperature profiles, $T(r) = T_0(L/L_\odot)^\alpha(r/r_0)^\beta$, for these grains as a function of stellar luminosity

TABLE 5
Model Fits to Spectra

Star	R_{BB} (AU)	T_{BB} (K)	R_1–R_2 (AU)	T_1–T_2 (K)	Optical Depth τ (10 μm)	Reduced χ^2	M_{grain} ($M_\oplus$)	($M_\oplus < 10$ km)
HD 7570	7.8 ± 0.8	98 ± 20	11–12	83–86	1.4×10^{-5}	0.68[a]	1.3×10^{-6}	0.042
HD 76151	8.1 ± 0.6	90 ± 14	7.6–8.7	93–86	21×10^{-5}	0.62[a]	1.6×10^{-6}	0.052
HD 128311	>15	<55	...	...	...	...	...	...
HD 206860	13.3 ± 1.2	73 ± 13	13.2–14.3	74–71	21×10^{-5}	0.5[a]	2.7×10^{-6}	0.087
HD 72905:								
0.25 μm silicate	...	...	0.03–0.43	1500–540	10×10^{-5}	...	7.2×10^{-10}	1.4×10^{-4}
	...	...	109–315	55–36	33×10^{-6}	0.83[b]	110×10^{-6}	22
10 μm silicate	14 ± 1	70 ± 10	12.2–15.9	67–63	7×10^{-5}	0.83[b]	3.3×10^{-6}	0.10

[a] $\lambda > 21$ μm, 74 dof.
[b] $\lambda > 8$ μm, 256 dof.

and distance from the central star by solving for the grain temperature at which the integrals over the absorbed stellar radiation and emitted thermal radiation were equal. The equilibrium temperature and power-law variation of temperature with distance and stellar luminosity depend on the assumed grain size and composition (Backman & Paresce 1993). As described below, we use 10 and 0.25 μm silicate grains (Draine & Lee 1984; Weingartner & Draine 2001) for which we obtained the following numerical relationships for large and small grains, respectively: $T(r) = 255\ \mathrm{K}(L/L_\odot)^{0.26}(r/\mathrm{AU})^{-0.49}$ and $T(r) = 362\ K(L/L_\odot)^{0.29} \times (r/\mathrm{AU})^{-0.41}$. These calculated coefficients and power-law constants closely follow analytical results (Backman & Paresce 1993).

We then calculated the dust excess by integrating over the surface brightness of a disk between R_1 and R_2, with $F_\nu(\lambda) = (2\pi/D^2)\int \tau_0(\lambda)(r/r_0)^{-p} B_\nu(T(r)) r\, dr$. In calculating the wavelength-dependent dust optical depth, $\tau(\lambda)$, we adopted grain emissivities Q_{abs} appropriate to small (0.25 μm) or large (10 μm) grains (Draine & Lee 1984; Weingartner & Draine 2001). The integrated surface density in the wedge-shaped disk expected for grains dominated by Poynting-Robertson drag is roughly uniform with radius, $p = 0$ (Burns et al. 1979; Buitrago & Mediavilla 1985; Backman 2004). We examined a number of other cases with $0 < p < 1$ that would reflect different dust dynamics, but did not find results that were substantially different from those for $p = 0$. Results of the model fitting are shown in Figure 4 and Table 5 and are discussed below.

Two other *Spitzer* studies have recently been published with results similar to those found here. Hines et al. (2006) identified a much younger (~30 Myr) star, HD 12039, with an IRS spectrum similar to that of HD 69830. Reporting on early results from the FEPS survey (Meyer et al. 2004), Kim et al. (2005) found a number of stars with 70 μm excesses with, in some cases, an accompanying excess in the IRS bands. The model results concerning the amount of dust and its orbital location are similar to those presented here.

5.1.1. *Single-Ring Models for HD 76151, HD 7570, HD 206860, and HD 128311*

For HD 7570, HD 206860, and HD 76151, which show no statistically significant, short-wavelength excess, we used only a single population of large, 10 μm, amorphous, silicate grains (Draine & Lee 1984; Weingartner & Draine 2001), fitting emission from a single annulus to 89 data points longward of 21 μm (just longward of the last point used for the flux normalization of the LL-1 IRS module) and including 70 μm. By varying τ_0, R_1, and R_2 we were able to minimize the reduced χ^2 to values between 0.5 and 0.8 with $77-3 = 74$ degrees of freedom (dof).

The models for HD 76151 and HD 7570 require grains with a narrow spread of temperatures around 100 K and located in the range of 7–10 AU. Assuming emission from only 10 μm grains, the predicted 850 μm flux density from the HD 7570 disk is well below the 1 mJy limit from SCUBA (Submillimeter Common-User Bolometric Array; J. Greaves 2005, private communication). The predicted 850 μm flux density from a disk containing larger (~100 μm) grains than this system would be approximately 1 mJy, just at the SCUBA limit. We cannot distinguish between the two grain sizes using only *Spitzer* data. HD 206860 has cooler grains (75 K) than the other stars with material located around 14 AU.

Mass estimates are notoriously tricky to derive given uncertainties in grain sizes, but these three systems suggest dust masses around $(1-2.6) \times 10^{-6}\ M_\oplus$ (Table 5) for a silicate grain density of 3.3 gm cm^{-3}. Extrapolating this estimate using the −3.5 index power law appropriate for a distribution of sizes from a collisional cascade (Dohnanyi 1969) up to a maximum size, R_{max}, of 10 km yields total mass estimates of 0.024–$0.080(R_{max}/10\ \mathrm{km})^{1/2}\ M_\oplus$. Submillimeter observations of all

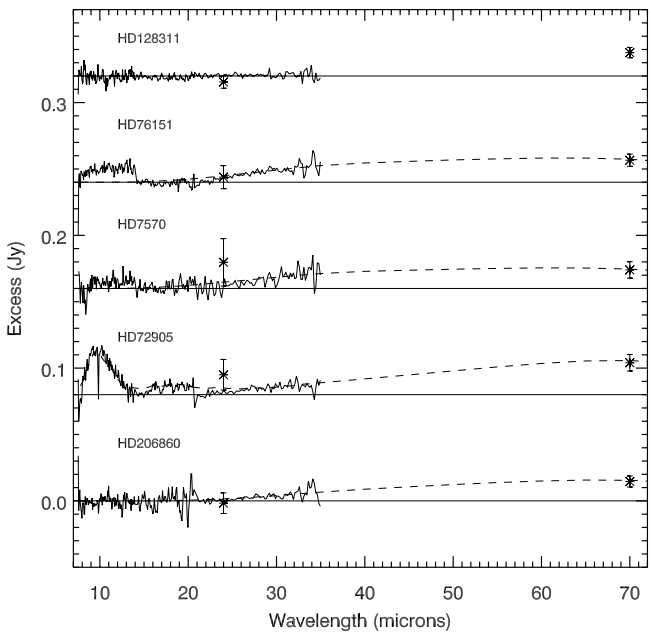

Fig. 4.—IRS spectra of those stars with excesses (*solid line*) along with their best fitting models (*dashed line*). The offset in SL-1 spectrum of HD 76151 is not statistically significant in terms of its fractional excess (1.4 σ). The spectrum of HD 69830, with its prominent IRS excess, is presented in Beichman et al. 2005b.

these sources would further constrain the dust size and distribution and thus the total mass of the emitting material.

Since the IRS data place only a limit on the emission shortward of 34 μm for the planet-bearing star HD 128311, the single-grain model can be used to show that the inner edge of the disk seen at 70 μm must start beyond $\sim$15 AU corresponding to material cooler than $\sim$50 K.

5.1.2. *Two Ring Model for HD 72905*

Since HD 72905 shows evidence for emission from small silicate grains starting around 8 μm, we separately examined three models: (1) small grains over a broad range of distances; (2) small grains in two annuli, one close to the star and one farther away; (3) small grains in a close-in annulus and large grains in a more distant annulus. For the small grains we used 0.25 μm grains composed of either amorphous silicates or crystalline forsterite (Malfait et al. 1998; Jäger et al. 1998). Unlike the dramatic case of HD 69830, small crystalline silicate grains provide a poor fit to the 8–14 μm data for this star (Fig. 4). Amorphous silicate grains have a broad emission profile particularly on the short-wavelength side, which appears in the HD 72905 spectrum but not in HD 69830's. A model providing a good fit to the data incorporates amorphous silicate grains located in an annulus extending from the grain sublimation distance (0.03 AU, corresponding to 1500 K) out to 0.43 AU, where the characteristic temperature is 500 K. The spectrum suggests an upper limit of no more than 10% of crystalline forsterite grains (by number).

However, this small dust population cannot extend out continuously much beyond 0.4 AU. Even with a density falloff proportional to $r^{-0.4}$ to r^{-1}, the presence of any dust between 1 and 10 AU produces far more radiation in the 20–70 μm region than is observed in the combined IRS+MIPS data. Thus we reject model 1 above. Rather, the data longward of 14 μm suggest a second population of cooler material located beyond 10 AU. We examined models with either small grains (0.25 μm, model 2) or large grains (10 μm, model 3) emitting at temperatures less than 90 K. Both models 2 and 3 give reasonable fits to the observations with reduced values of $\chi^2 \sim 0.8$. As Table 5 indicates, a much greater quantity of small grains emitting at cooler temperatures is required to fit the data compared to a model using larger grains. This difference is due to the greatly reduced emissivity of small 0.25 μm versus large 10 μm grains, e.g., at 70 μm, $Q_{\rm abs} = 0.008$ versus 1.84 (Draine & Lee 1984; Weingartner & Draine 2001).

A testable difference between the large- and small-grain models is the size of the emitting region. For small grains, the emitting annulus extends between 109 and 310 AU, corresponding to a diameter of 40″ at the 14.1 pc distance to the star. By contrast, large grains cool more efficiently and are located closer to the star, <16 AU, for a predicted diameter of only 2″. Since there is no evidence that the 70 μm image of HD 72905 is extended, we favor the large-grain model. The total amount of material in the HD 72905 disk is about a factor of 2 greater than in the other disks studied here.

5.2. *Nature of Disks*

5.2.1. *Rarity of Emission from Warm Dust*

The vast majority of the stars studied here, planet-bearing or not, have no emission interior to $\sim$10 AU at the levels to which IRS is sensitive, 75–1400 times that of our zodiacal cloud. Since this result applies equally to stars with and without planets, there must be some general explanation for the absence of warm material around mature stars >1 Gyr). A long-term decline in the amount of debris expected on theoretical grounds (Dominik & Decin 2003) and demonstrated with the envelope of the distribution of 24 μm excesses seen in A stars, implying an excess $\propto 150\ {\rm Myr}/t_{\rm Myr}$ (Rieke et al. 2005), is consistent with the results of this survey. Modifying equations (35)–(40) of Dominik & Decin (2003) for parameters appropriate to an asteroid belt located between 1 and 5 AU leads to the conclusion that after one billion years, $L_{\rm dust}/L_\star$ in the IRS wavelength range should be $\leq 10^{-6}$ and thus undetectable with IRS over a broad range of initial conditions.

Three of the disks (HD 7570, HD 206860, and HD 76151) have an inner edge around $\sim$10 AU and may be only a few AU wide (Table 5). The cutoff at wavelengths shorter than $\sim$25 μm corresponds to temperatures <75–100 K and location $\geq$7 AU. Other stars observed in this or other *Spitzer* programs with 70 μm excess that do *not* show an inner emission cutoff at 25 μm seem to have some extenuating circumstance: Vega, with evidence for a recent collision (Su et al. 2005); β Pic, which is extremely young; Fomalhaut (Stapelfeldt et al. 2004); two young stars, HD 72905 and HD 12039 (Hines et al. 2006); and HD 69830 (Beichman et al. 2005b), with a sharply bounded, interior dust belt originating, perhaps, in an active asteroid belt. If the observational trend for a general lack of material interior to $\sim$10 AU continues as more *Spitzer* data accumulate, then it may be that this inner boundary to the "Kuiper belt" is related to the ice-sublimation distance $\geq 3L_\star^{0.5}$ AU, where significant amounts of material could have accumulated in the protoplanetary disk (Thommes et al. 2003).

The amount of warm material around HD 72905 with $L_{\rm dust}/L_\star \sim 13 \times 10^{-5}$ (cf. Table 4) is well above values consistent with the simple models (Dominik & Decin 2003), even given the relative youth of this star ($\sim$0.3 Gyr). The excess may be attributable to a recent collisional event between planetesimals, as has been suggested by Kenyon & Bromley (2004a) and Rieke et al. (2005) for A stars observed at 24 μm. As discussed in Beichman et al. (2005b), the disk of hot, small grains around a mature star, HD 69830, stands out as exceptional in this survey and may similarly be the result of a rare transient event in an unusually massive asteroid belt. In the case of steady state emission (rather than transient events), the brightness of an excess will be proportional to the first or second power of the number of colliding planetesimals, depending on whether the ultimate loss mechanism for the smallest grains is blowout by radiation pressure or PR-drag, respectively (Dominik & Decin 2003). Since PR-drag is likely to be more effective than blowout for the low-luminosity stars considered here (Sheret et al. 2004), a 74–1400-fold brighter zodiacal cloud than our own would imply the existence of (or a limit to) an asteroid belt $\sqrt{75}$–$\sqrt{1400} \sim 8$–35 times more massive than our own, depending on its location. The results of this IRS survey suggest that asteroid belts of such a large mass are rare around mature, solar-type stars.

As pointed out by an anonymous referee, there are alternatives to the transient collision hypothesis for the origin of the debris disks around mature stars. Stirring up a quiescent asteroid or Kuiper belt by planetary migration caused by either orbital interactions (Gomes et al. 2005; Strom et al. 2005) or to the effects of a passing star (Kenyon & Bromley 2004b) has been suggested as possible causes for analogs of the period of late heavy bombardment in our solar system. A strong infrared excess could be a signpost of a similarly exciting period in other planetary systems. For the young stars HD 72905 (this survey) and HD 12039 (Hines et al. 2006), this analogy is quite plausible. On the other hand, for the older stars in this survey, including the >2 Gyr-old HD 69830, it is not clear that planetary migration is likely so

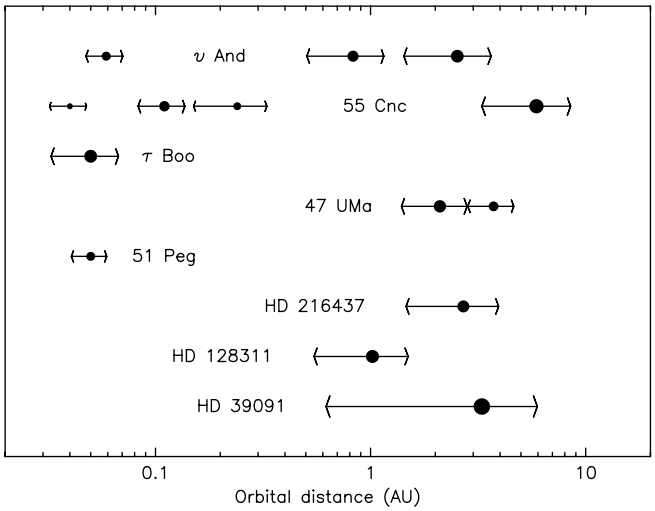

FIG. 5.—For each star with planets the minimum and maximum extents of the gravitational influence of that star's planets are plotted. The lack of emission in the IRS wavelength region is consistent with a dearth of material interior to about 5 AU. A partial explanation may be the influence of planets on dust in disks.

long after the formation of these planetary systems. Confirmation of this hypothesis will require a more complete census of planetary systems than is at present available.

5.2.2. *Lack of Warm Dust and the Presence of Planets*

None of the planet-bearing stars show an IRS excess, and only one, HD 128311, shows a MIPS excess. We assume that the gravitational influence of a planet at orbital semimajor axis, a_p, and eccentricity, ϵ_p, is given by $r_{\rm grav} \sim (\epsilon_p^2 a_p^2 + 12R_{\rm Hill}^2)^{1/2}$, where the Hill radius is defined as $R_{\rm Hill} = a_p[M_p/(3M_*)]^{1/3}$ (Bryden et al. 2000) with M_p and M_* the masses of planet and star. As shown in Figure 5, the region between $R_{\rm min} = a - r_{\rm grav}$ and $R_{\rm max} = a + r_{\rm grav}$ could be swept clean of dust due to sweeping up action by the planet.[6] In addition to more global effects leading to a general decline in dust content, as discussed in the preceding section, gravitational effects of planets in relatively distant orbits (HD 39091, 55 Cnc, 47 UMa, HD 216437, and υ And) might clear out the material interior to $\sim$10 AU in the absence of a secondary source such as a massive asteroid belt. Stars with close-in planets (τ Boo and 51 Peg) may require another explanation (or an as yet undetected, more distant planet) for the lack of material in the 1–10 AU region.

[6] Planet properties from Planet Encyclopedia at http://cfa-www.harvard.edu/planets.

6. CONCLUSION

We have used the IRS spectrometer on the *Spitzer Space Telescope* to look for weak excesses around main-sequence, solar-type stars. After careful calibration, the IRS spectra allow us to achieve relatively low values of $L_{\rm dust}/L_\star$ compared to previous studies. At 8–13 μm the IRS data provide an average 3 σ limit of $L_{\rm dust}/L_\star = 14 \pm 6 \times 10^{-5}$ or roughly 1400 times the level of our solar system zodiacal cloud for material in the 1 AU region of the target stars. Two stars, HD 72905 and HD 69830, have detectable emission at these wavelengths, and in both cases there is evidence for emission by small dust grains. At 30–34 μm, we reach a more sensitive, limit on $L_{\rm dust}/L_\star$ of $0.74 \pm 0.31 \times 10^{-5}$, or roughly 74 times the level of our solar system zodiacal cloud for material in the 5–10 AU region, which may represent the inner edge of the Kuiper Belt. Four stars (HD 7570, HD 72905, HD 76151, and HD 206860) showed evidence for long-wavelength IRS emission that appears to link smoothly to a 70 μm MIPS excess. HD 69830 shows no evidence for 70 μm excess and thus for colder, more distant material.

The lack of IRS excess emission toward planet-bearing stars may be due to the small size of the sample observed to date, to the effects of planets removing dust from the orbital locations probed at IRS wavelengths, or to more general processes that remove dust from regions interior to a few AU (Dominik & Decin 2003). We suggest that asteroid belts located between 1 and 10 AU and as massive as 8–35 times our own asteroid belt are rare around mature, solar-type stars.

Sergio Fajardo-Acosta provided the programs we used for accessing the Kurucz models. This research made use of the *IRAS*, *2MASS*, and *Hipparcos* (VizieR Online Data Catalog, 1239) catalogs, as well as the SIMBAD database and the VizieR tool operated by CDS, Strasbourg, France. We gratefully acknowledge the comments of an anonymous referee whose careful reading of the manuscript led to a number of useful points of discussion and clarification.

The *Spitzer Space Telescope* is operated by the Jet Propulsion Laboratory, California Institute of Technology, under NASA contract 1407. Development of MIPS was funded by NASA through the Jet Propulsion Laboratory, subcontract 960785. Some of the research described in this publication was carried out at the Jet Propulsion Laboratory, California Institute of Technology, under a contract with the National Aeronautics and Space Administration.

Finally, we remember with great sadness the efforts of NRC postdoctoral fellow Elizabeth Holmes who worked intensively on this project before her untimely death in 2004 March.

APPENDIX

DETAILS OF IRS DATA REDUCTION

Standard IRS Staring mode observations were made with the Short-Low Order 1 (SL1; 7–14 μm), Long-Low Order 2 (LL-2; 14–20 μm), and Long Low Order 1 (LL-1; 20–35 μm) modules. Each star was observed at two positions along the slit, called $\rm Nod_1$ and $\rm Nod_2$. Data were processed by the *Spitzer* Science Center (SSC) to produce calibrated images of the spectrometer focal plane. The data presented here were processed with version 11.0 of the SSC pipeline (2005 February). The SSC SPICE software was used to extract spectra from the images. Because of the need for careful subtraction of the stellar continuum to detect a faint excess, additional steps were taken in producing the final spectra. These are now described briefly.

The first few points at the beginning and end of the spectrum from each module were typically unreliable, as were a few bad pixels flagged in the SSC processing. These data were rejected. This effect was particularly noticeable at the long-wavelength end of SL1 ($\lambda > 14$ μm). However, since the short-wavelength end of LL-2 overlaps SL1, there is no gap in the final spectrum.

Longward of $\sim$7 μm, the photospheres of solar-type stars are smooth and do not differ greatly from a Rayleigh-Jeans blackbody curve (Kurucz 1992; Castelli & Kurucz 2003). We used this fact to improve the pixel-to-pixel calibration in the extracted SSC/SPICE spectra. Of the 41 stars listed in Table 1, 28 stars showed no clear evidence for an excess at either 24 or 70 μm with MIPS or with the initial pass of IRS processing but did show consistent pixel-to-pixel deviations from a smooth photospheric model.

For these stars we formed ratios of the extracted IRS spectra to the Kurucz model appropriate for the effective temperature and metallicity of each star. From the average of these ratios at each wavelength, we created a superflat response curve for the SL1, LL-2 and LL-1 modules. Only those stars which did not show signs of an excess during the initial pass of the data were included in the superflat. Shortward of 14 μm, the SL1 superflat typically has values in the range 0.97–1.03, or, equivalently, deviations from unity response of $\sim$3%; a few pixels have values deviating from unity by 10%. The values at each pixel of the SL1 superflat have a dispersion around the pixel response (averaged over 28 stars showing no signs of excess in IRS or MIPS data) of $\sigma_{\rm pop} \sim 2\%$ and $\sigma_{\rm mean} \sim 0.4\%$. In the LL-1 and LL-2 modules, the typical superflat values are in the range 0.98–1.02, with dispersions of $\sigma_{\rm pop} \sim 1\%-2\%$ and $\sigma_{\rm mean} \sim 0.2\%-0.3\%$. We divided the extracted spectra by the appropriate superflat to remove any residual calibration variations. The dispersion in the superflat ($\sigma_{\rm pop}$) is an indication of the limiting systematic noise in removing the photospheric contribution to the signal from these stars.

Although the spectrum of HD 101501 shows no excess at the $\sim$10% level in either the MIPS or IRS data, its spectrum did not behave in a consistent manner when the various normalization steps were applied to look for fainter excesses. Differential pointing issues or other time variable effects could have produced a spectrum deviating from the mean for nonastrophysical reasons. The module-wide deviations from flatness are suggestive of uncorrected flat-field errors, not astrophysical effects. As a result, this star was excluded from the generation of the superflat.

The comparison between the SSC spectra and the photospheric models fitted to shorter wavelength photometry (Bryden et al. 2006) shows absolute calibration gain factors of F_ν(SSC)/F_ν(photospheric model) $= 0.84 \pm 0.01$ (5% dispersion from star to star) in the LL-1 and LL-2 modules and 1.12 ± 0.014 (7% dispersion from star to star) in the SL-1 module. As discussed in § 3.1 the agreement between IRS data and *IRAS* or MIPS observations is excellent with deviations from unity of 4% $\pm$ 1% at 12 μm, 7% $\pm$ 1% at 24 μm (consistent with a known calibration issue with *IRAS* data at this wavelength; e.g., Cohen et al. 1992), and 1% $\pm$ 1% at MIPS-24 μm.

REFERENCES

Aumann, H. H., & Probst, R. G. 1991, ApJ, 368, 264
Aumann, H. H., et al. 1984, ApJ, 278, L23
Backman, D. E. 2004, in ASP Conf. Ser. 324, Debris Disks and the Formation of Planets: A Symposium in Memory of Fred Gillett, ed. L. Caroff et al. (San Francisco: ASP), 9
Backman, D. E., Dasgupta, A., & Stencel, R. E. 1995, ApJ, 450, L35
Backman, D. E., & Paresce, F. 1993, in Protostars and Planets III, ed. V. Mannings, A.P. Boss, & S. S. Russell (Tucson: Univ. Arizona Press), 1253
Beichman, C., et al. 2005a, ApJ, 622, 1160
———. 2005b, ApJ, 626, 1061
Bryden, G., Lin, D. N. C, & Ida, S. 2000, ApJ, 544, 481
Bryden, G., et al 2006, ApJ, 636, 1098
Buitrago, J., & Mediavilla, E. 1985, A&A, 148, L8
Burns, J., Lamo, P. L., & Soter, S. 1979, Icarus, 40, 1
Butler, R. P., Marcy, G. W., Fischer, D. A., Brown, T. M., Contos, A. R., Korzennik, S. G., Nisenson, P., & Noyes, R. W. 1999, ApJ, 526, 916
Castelli, F., & Kurucz, R. L. 2003, IAU Symp. 210, Modelling of Stellar Atmospheres, ed. N. E. Piskunov, W. W. Weiss., & D. F. Gray (San Francisco: ASP), 20
Cohen, M., Walker, R. G., Barlow, M. J., & Deacon, J. R. 1992, AJ, 104, 1650
Dermott, S. F., Kehoe, T. J. J., Durda, D. D., Grogan, K., & Nesvorný, D. 2002, in Asteroids, Comets, and Meteors, ed. B Warmbein (ESA SP-500; Noordwijk: ESA), 319
Dohnanyi, J. S. 1969 J. Geophys. Res., 74, 2431
Dominik, C., & Decin, G. 2003, ApJ, 598, 626
Draine, B. T., & Lee, H. M. 1984, ApJ, 285, 89
Fajardo-Acosta, S., Beichman, C., & Cutri, R. 2000, ApJ, 538, L155
Gomes, R., Levison, H. F., Tsiganis, K., & Morbidelli, A. 2005, Nature, 435, 466
Gordon, K. D., et al. 2005, PASP, 117, 503
Hines, D., et al. 2006, ApJ, in press
Houck, J. R., et al. 2004, ApJS, 154, 18
Jäger, C., Molster, F. J., Dorschner, J., Henning, Th., Mutschke, H., & Waters, L. B. F. M, 1998, A&A, 339, 904
Kenyon, S. J., & Bromley, B. C. 2004a, ApJ, 602, L133
———. 2004b, Nature, 432, 598
Kim, J. S., et al, 2005, ApJ, 632, 659
Kurucz, R. L. 1992, in IAU Symp. 149, The Stellar Populations of Galaxies, ed. B. Barbuy & A. Renzini (Dordrecht: Kluwer), 225
Laureijs, R. J., et al. 2002, A&A, 387, 285
Malfait, K., Waelkens, C., Waters, L. B. F. M., Vandenbussche, B., Huygen, E., & de Graauw, M. S. 1998, A&A, 332, L25
Mannings, V., & Barlow, M. J. 1998, ApJ, 497, 330
Marcy, G. W., Butler, R. P., Fischer, D. A., Laughlin, G., Vogt, S. S., Henry, G. W., & Pourbaix, D. 2002, ApJ, 581, 1375
Meyer, M., et al. 2004, ApJS, 154, 422
Rieke, G. H., et al. 2004, ApJS, 154, 25
———. 2005, ApJ, 620, 1010
Sheret, I., Dent, W. R. F., & Wyatt, M. C. 2004, MNRAS, 348, 1282
Spangler, C., Sargent, A. I., Silverstone, M. D., Becklin, E. E., & Zuckerman, B. 2001, ApJ, 555, 932
Stapelfeldt, K., et al. 2004, ApJS, 154, 458
Stern, A. S. 1996, A&A, 310, 999
Strom, R. G., Malhotra, R., Ito, T., Yoshida, F., & Kring, D. A. 2005, Science, 309, 1847
Su, K., et al. 2005, ApJ, 628, 487
Thommes, E. W., Duncan, M. J., & Levison, H. F. 2003, Icarus, 161, 431
Weingartner, J. C., & Draine, B.T. 2001, ApJ, 548, 296